

FAST AND AUTOMATIC SKULL SEGMENTATION OF MULTIDETECTOR CT HEAD IMAGES

Petr Walek

Doctoral Degree Programme (2), FEEC BUT

E-mail: walek@feec.vutbr.cz

Supervised by: Jiří Jan

E-mail: jan@feec.vutbr.cz

Abstract: This paper describes automatic and fast skull segmentation of head X-ray computed tomography (X-ray CT) images. Acquired data suffers from salient stair-step artifact which is corrected by registration using combination of phase correlation and gradient descent optimization methods. Skull segmentation is performed in the two steps, the first is segmentation of cortical bones by means of simple thresholding, and the second is classification of trabecular bones utilize information about shape of local histograms.

Keywords: X-Ray Computed Tomography, Stair-Step Artifact Correction, Skull Segmentation

1 INTRODUCTION

Segmentation of bones in images acquired by X-ray CT is a challenging task in a field of medical image processing, especially the segmenting of a basis cranii, a very complex bony structure a in bottom of a skull. Many new algorithms and approaches have been recently proposed in this field, see [1], [2]. Segmentation of skull is currently used in many tasks such as image guided surgery, detection of fractures, image registration ect. therefore faster and more reliable automatic algorithms are still needed.

2 CORRECTION OF A STAIR-STEP ARTIFACT

Acquired images of head suffers from the very severe stair-step artifact, especially after reformatting to a sagittal plane, as can be clearly seen in Fig. 2a. In general a stair-step artifact is caused by using wide collimation and a non-overlapping reconstruction interval [3] especially using multisection scanning. Artifact introduces translational shift into sub-volumes identically located according to sections acquired on the one gantry rotation during multisection scanning. Such shifts are capable to preclude further processing and analysis of segmented bones or harm the process of bones segmentation.

2.1 POSITIONAL DETECTION OF TRANSLATED SUB-VOLUMES MARGINS

The first step in correction of the stair-step artifact is positional detection of margins of displaced sub-volumes. Positions of marginal slices are detected by evaluation of the Euclidean distance similarity function (1), computed between consecutive slices. Variables \mathbf{a} and \mathbf{b} in this equation means pixel intensities rearranged to a vector and N is a number of pixels in images.

$$C_E(\mathbf{a}, \mathbf{b}) = \sqrt{\sum_{i=0}^N (a_i - b_i)^2} \quad (1)$$

Resulting vector of Euclidean distances as a function of slice positions can be seen in Fig. 1a. Despite of clearly visible peaks in the similarity function there is also a slow and strong trend which can

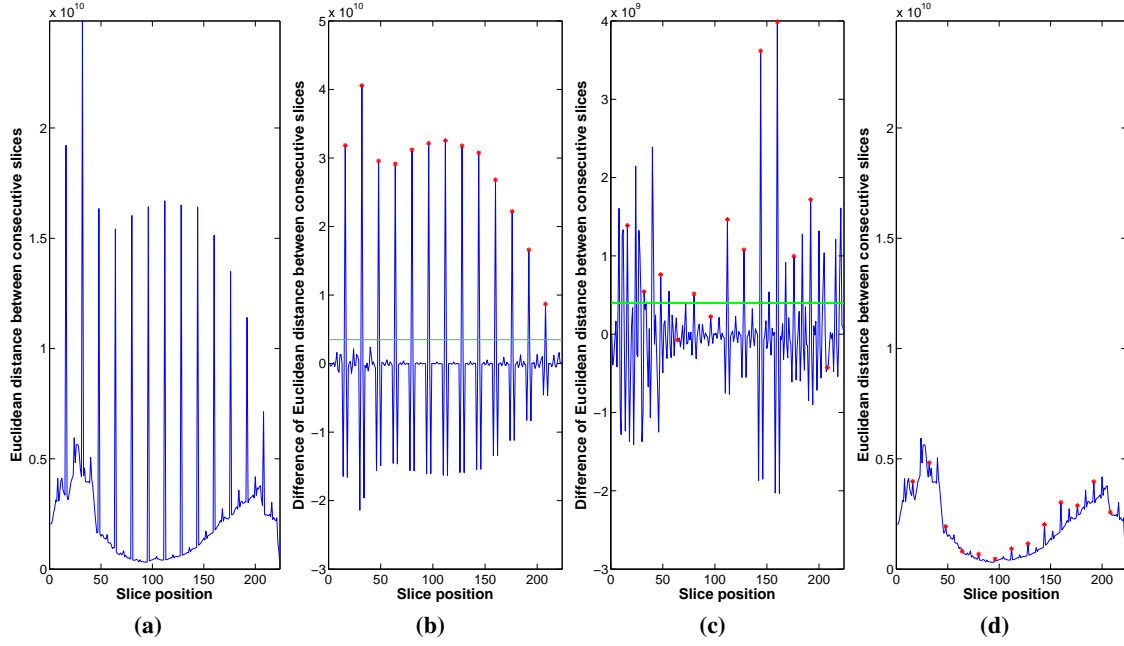


Figure 1: Euclidean distance between consecutive slices (EDCS): (a) original image, (b) difference of EDCS with detected marginal slices (red stars) and threshold (green line), (c) difference of EDCS after registration using phase correlation, (d) EDCS of finally corrected image

possibly preclude the detection, and is removed by differentiation of this curve. Resulting difference of the similarity function can be seen in Fig. 1b and a peaks detection algorithm is applied on it (note that as a peak is labeled each position in the vector with a bigger value than their neighbors). Detected peaks are thresholded, threshold is determined as the mean of absolute values of the vector (depicted as a green line), thereby the most significant peaks, representing positions of the most dissimilar consecutive slices, are obtained. The last step is a determination of a patient table translational increment after the one rotation of a gantry which corresponds with sizes of mutually translated sub-volumes. Translational increment of patient table is computed as the median of vector containing distances between the neighboring detected peaks. Finally detected margins of sub-volumes are plotted in Fig. 1b as red stars.

2.2 REGISTRATION OF DISPLACED SUB-VOLUMES

Once positions of mutually translated sub-volumes margins are know registration of sub-volumes is performed. Taking into account a character of the stair-step artifact (a simple translation of sub-volumes) phase correlation technique, originally proposed in [4], is chosen as a basis for registration. This method is based on a Fourier shift property stating that a planar shift between two functions is expressed in a Fourier domain as a linear phase difference. Lets have two functions $f_1(x, y)$, $f_2(x, y)$ and suppose that they varies only by a translation about Δx and Δy

$$f_2(x, y) = f_1(x - \Delta x, y - \Delta y). \quad (2)$$

According to a Fourier shift property equation 2, can be restated to

$$F_2(u, v) = F_1(u, v) \cdot e^{-i(u \cdot \Delta x + v \cdot \Delta y)}, \quad \text{where } F_i(u, v) = DFT_{2D}(f_i(x, y)), \quad (3)$$

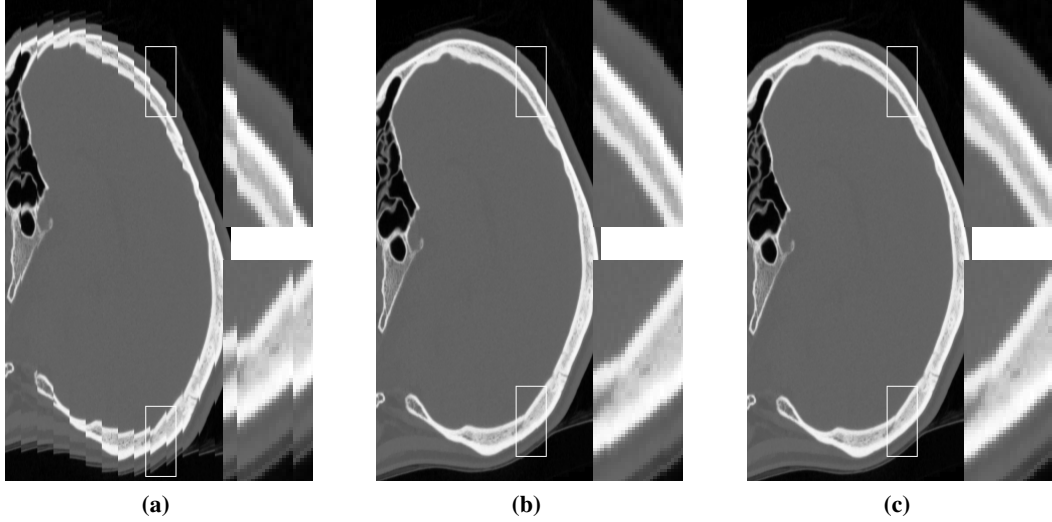


Figure 2: Slices of X-ray CT images reformatted to a sagittal plane (with magnified sections): (a) original slice, (b) slice after registration by phase correlation, (c) slice after registration by gradient descent optimization.

and shifting of image thus do not influence its amplitude spectrum. Phase correlation can be calculated as a Fourier transform of a normalized cross power spectrum

$$p(x,y) = DFT_{2D}^{-1} \left[\frac{F_2(u,v) \cdot F_1(u,v)^*}{|F_2(u,v) \cdot F_1(u,v)|} \right]. \quad (4)$$

This phase correlation matrix contains a strong impulse in position $[\Delta x, \Delta y]$ which is detected as the strongest peak. Vector of translation parameters $[\Delta x, \Delta y]'$ for each sub-volume is known and alignment can be performed in a very simple manner as $[x, y]' + [\Delta x, \Delta y]'$. Phase correlation, in its basic form, cannot determine sub-pixel shifts and registration therefore can not be sufficient, see Fig. 2b. After registration of sub-volumes by phase correlation, difference of Euclidean distance between consecutive slices is computed and thresholded again Fig. 1c. Euclidean distances between sub-volumes margins (labeled as red stars) above threshold are then minimized by gradient descent optimization method, providing final correction of stair-step artifact, see Fig. 2c and Fig. 1d.

3 SEGMENTATION OF SKULL

Segmentation of skull is carried out in the two main steps, segmentation of cortical bones and classification of trabecular bones. Cortical bone is a dense part of bone forming its surface while trabecular bone is denomination of its internal part which is less dense than cortical bone.

3.1 SEGMENTATION OF CORTICAL BONES

The simplest and fastest method for segmenting cortical bones parts is intensity thresholding. A threshold is needed for this operation and probably the best way for its automatic determination is evaluation of the image histogram.

A typical brightness histogram of the whole brain volume comprises only two distinct peaks, and can be seen in Fig. 3 plotted as a blue bar graph, note that pixel intensities are normalized to be in interval $\langle 0, 1 \rangle$. The peak situated at lower intensities belongs to representation of surrounding air and sinuses, while second significant peak belongs to a representation of soft tissue. Intensities belonging to bones are spread over a wide range hence there is no distinct, detectable peak. Threshold for cortical bones

segmentation is therefore derived from a position of soft tissue peak which is detected in similar way as peaks in chapter 2. Peak with the second highest value is considered to be representation of soft tissue. Detected position of the soft tissue peak serves as a mean μ and magnitude as parameter a of initial Gaussian function 5 used to approximate properties of soft tissue lobe (variance σ is initially selected as 0.01).

$$f(x) = a.e^{-0.5\left(\frac{x-\mu}{\sigma}\right)^2} \quad (5)$$

The initial Gaussian curve is depicted in Fig. 3 (please notice detailed plot) by the red curve and is optimized by a least-squares curve fitting algorithm in order to find optimal parameters μ and σ (green curve in Fig. 3). Threshold for bone segmentation is empirically determined as $\mu + 20.\sigma$ (black line in Fig. 3). In this way the threshold for bones segmentation is determined automatically and independently on the input data.

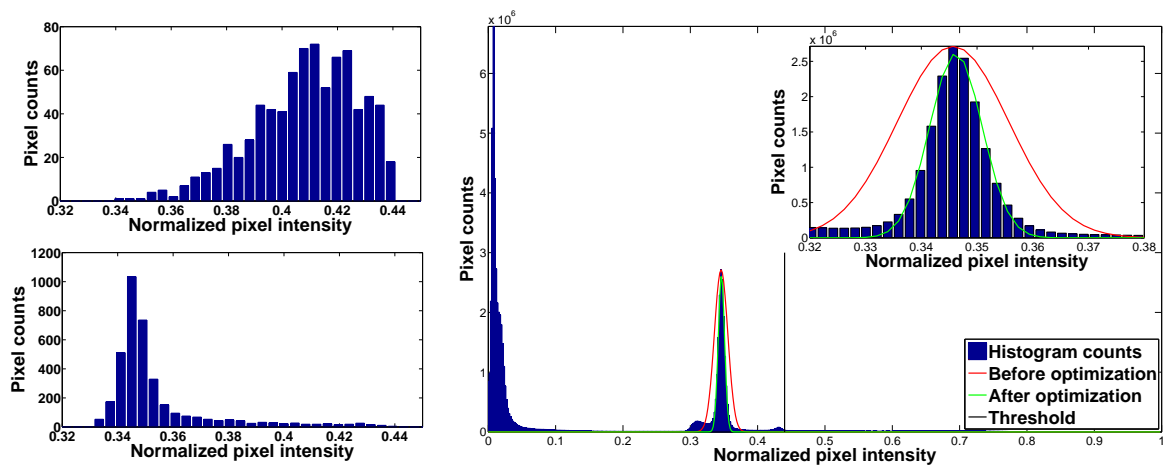


Figure 3: Right: Histogram of the whole head volume, upper left: typical histogram of the hole labeled as trabecular bone, bottom left: typical histogram of the hole labeled as soft tissue

3.2 CLASSIFICATION OF TRABECULAR BONES

Intensities (i.e. Hounsfield units or tissue density) in trabecular parts of bones are partially overlapped with intensities of soft tissue, therefore simple thresholding is only capable to segment cortical parts of bones as can be seen in Fig. 4b (note that resulting binary masks 4b and 4d are in this view multiplied with the original slice 4a) and because of that empty spaces (in this paper called “holes”) appears instead trabecular parts of bones. Separation of holes by a boundary tracking technique (Fig. 4c) is therefore next step followed by decision if particular hole presents soft tissue or trabecular bone.

As stated before intensities of soft tissue and trabecular bones are partially overlapping, nevertheless their intensity histograms differ in shape, typical histograms for soft tissue hole and trabecular bone are depicted in Fig. 3. Histograms of trabecular bones parts are, in comparison with soft tissue ones, more compact (histogram counts are smoother) and skewed towards higher intensities. Shape of a particular histogram is objectified by five parameters: entropy 7, compactness 8, relative position of the histogram mean according to position of soft tissue peak in histogram of whole volume 6, skewness 9 and kurtosis 10. In each of the following equations N means sum of all counts in bins (i.e. number of pixels in hole), i is a bin mark and x_i means counts in the bin marked as i .

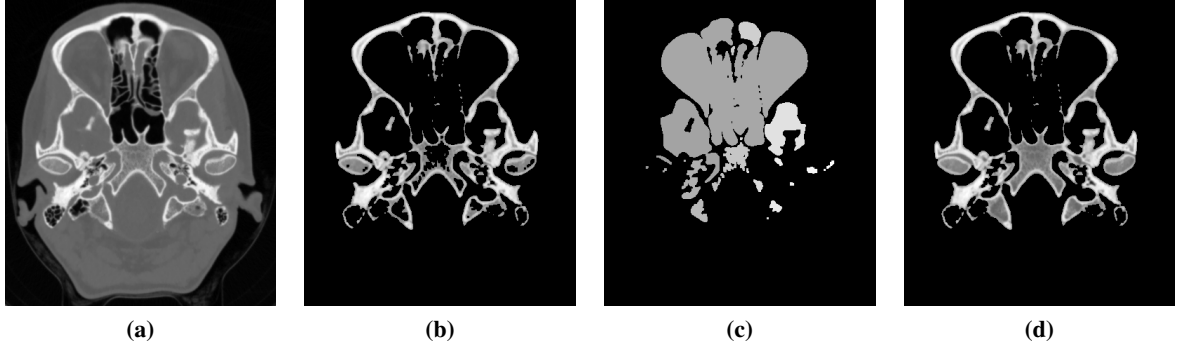


Figure 4: Skull segmentation: (a) original slice, (b) cortical bones segmentation, (c) holes extracted by boundary tracking, (d) final bones segmentation

$$P_{rel} = \frac{P_{pos}}{\mu}, \quad \text{where} \quad \mu = \frac{1}{N} \sum_{i=0}^{n-1} x_i i. \quad (6)$$

$$S = -\frac{1}{N} \sum_{i=0}^{n-1} x_i \log(x_i). \quad (7) \quad C = \frac{1}{N} \sum_{i=0}^{n-1} \frac{x_i}{\max(x)} \quad (8)$$

$$\gamma_1 = \frac{\frac{1}{N} \sum_{i=0}^{n-1} (i - \mu)^3}{\left[\frac{1}{N} \sum_{i=0}^{n-1} (x_i i)^2 - \mu^2 \right]^{\frac{3}{2}}}. \quad (9) \quad \gamma_2 = \frac{\frac{1}{N} \sum_{i=0}^{n-1} (i - \mu)^4}{\left[\frac{1}{N} \sum_{i=0}^{n-1} (x_i i)^2 - \mu^2 \right]^2} - 3. \quad (10)$$

Classification of the holes is done by a simple neural network, trained by set of 300 exemplary vectors, each vector is composed of histogram parameters resulting from equations 6 - 10. Each exemplary vector is manually classified and this classification is verified by an experienced radiologist. Final segmentation of bones in complex structure of basis cranii can be seen in Fig. 4d.

4 CONCLUSIONS

Stair-step artifact and fast, automatic segmentation of skull are presented in this paper. Correction of artifact provides satisfactory results combining phase correlation and gradient descent optimization registration. Segmentation of typical head volume (512x512x224 voxels) takes only 15 seconds on workstation with 2x Intel Core i7 CPU (3.4GHz) with 16GB RAM, using MATLAB environment.

REFERENCES

- [1] Y. Kang, K. Engelke, and W. Kalender, "A new accurate and precise 3-D segmentation method for skeletal structures in volumetric CT data.," IEEE transactions on medical imaging, vol. 22, no. 5, pp. 586-98, May 2003.
- [2] X. Zang, Y. Wang, J. Yang, and Y. Liu, "A novel method of CT brain images segmentation," International Conference of Medical Image Analysis and Clinical Application, 2010, pp. 109-112.
- [3] J. F. Barrett and N. Keat, "Artifacts in CT: recognition and avoidance," Radiographics: a review publication of the Radiological Society of North America, Inc, vol. 24, no. 6, pp. 1679-91, 2004.
- [4] C. D. Kuglin and D. C. Hines, "The phase correlation image alignment method," in Proc. Int. Conf. Cybernetics Society, pp. 163-165, 1975.